Phylloquinone and Related Radical Anions Studied by Pulse Electron Nuclear Double Resonance Spectroscopy at 34 GHz and Density Functional Theory

Boris Epel,[†] Jens Niklas,[†] Sebastian Sinnecker,[†] Herbert Zimmermann,[‡] and Wolfgang Lubitz*,[†]

Max-Planck-Institut für Bioanorganische Chemie, Stiftstrasse 34-36, D-45470 Mülheim/Ruhr, Germany, and Max-Planck-Institut für Medizinische Forschung, Jahnstrasse 29, D-69120 Heidelberg, Germany

Received: January 25, 2006; In Final Form: March 10, 2006

^{1}H hyperfine (hf) coupling constants of semiquinone radical anions of 1,4-naphthoquinone, 2-methyl-1,4-naphthoquinone, and 2-methyl-3-phytyl-1,4-naphthoquinone in frozen alcoholic solutions were measured using pulse Q-band electron nuclear double resonance spectroscopy. The resolved signals of the quinone protons as well as from hydrogen bond and solvent shell protons were analyzed and assigned. Both in-plane and out-of-plane hydrogen bonding with respect to the π-plane of the radical is observed. Interactions with nonexchangeable protons from the surrounding matrix are detected and assigned to solvent protons above and below the quinone plane. Density functional theory was used to calculate spin Hamiltonian parameters of the radical anions. Solvent molecules of the first solvent shell that provide hydrogen bonds to the quinones were included in the geometry optimization. The conductor-like screening model was employed to introduce additional effects of the solvent cage. From a comparison of the experimental and calculated hf tensors it is concluded that four solvent molecules are coordinated via hydrogen bonds to the quinone oxygens. For all radicals very good agreement between experimental and calculated data is observed. The influence of different substituents on the spin density distribution and hydrogen bond geometries is discussed.

Introduction

Vitamin K plays an important role in physiological processes of many organisms. In mammals it is used to control blood clotting and bone formation and assists in converting glucose to glycogen in the intestines.[1] In plants and bacteria it is, for example, involved in electron transfer in photosynthesis.[2−4] In nature two types of vitamin K are found. Vitamin K_1 (VK_1), also called phylloquinone, is found in plants and cyanobacteria.[2,5] Vitamin K_2 is a collective term for a group of compounds, called menaquinones (MQs), synthesized by anoxygenic bacteria.[6] They differ from VK_1 with respect to the length and structure of the chain attached to position 3 of the quinone ring. There are also artificial forms, vitamin K_3 (VK_3), menadione, and vitamin K_4, called menadiol.

In photosystem I (PS I) VK_1 serves as an intermediate acceptor (named A_1) in the electron transport across the photosynthetic membrane. During the electron transfer the phylloquinone is singly reduced, and the semiquinone radical anion is formed.[7−9] A menaquinone has a similar function in anoxygenic photosynthesis.[6,10,11] The specific binding of the quinone to the protein modifies its electronic structure and properties. For example, the redox potential of A_1 is several hundred millivolts more negative than the potential of VK_1 in water.[12,13]

Since electron paramagnetic resonance (EPR) can directly probe the electronic structure, it is the method of choice for studying radicals. Due to the importance of understanding the quinone function in biological systems a large number of EPR studies have been performed in the past, e.g., refs 8, 9, 11, and 14−16. Since natural systems are often not easily accessible to experimental and theoretical studies, model compounds, which mimic the properties of their biological counterparts, are widely used to understand the function of protein-bound cofactors. This study focuses on the chemically formed semiquinone radical anions $NQ^{\bullet-}$, $VK_3^{\bullet-}$, and $VK_1^{\bullet-}$. 1,4-Naphthoquinone (NQ) is a simple structural analogue of vitamin K without substituents. NQ and VK_3 have been recently incorporated into the A_1 binding site of PS I and investigated as electron transport cofactors.[8,17]

An important parameter that characterizes the electronic structure of radicals is the *g*-tensor. Quinone radicals show only a small *g*-anisotropy, which is often not resolved at conventional (X-band) frequencies. At higher frequencies the *g*-anisotropy can frequently be resolved, and all principal components of the *g*-tensor can be obtained.[18,19] Further insight is provided by electron nuclear double resonance (ENDOR) spectroscopy,[20−22] from which the hyperfine coupling constants (hfcc's) of magnetic nuclei can often be obtained even for complicated radicals in frozen solutions. ENDOR experiments can be done in continuous wave (CW) or pulsed mode. Both methods have specific advantages and are thus complementary. CW ENDOR experiments in liquids[21] allow the direct determination of the isotropic hfcc due to motional averaging of the anisotropic part of the hf interaction in solution. However information on the dipolar interaction is not available from liquid solution ENDOR.

In frozen solution CW ENDOR suffers from low sensitivity, relaxation dependence of ENDOR efficiency, and baseline problems. Therefore, pulse ENDOR is the method of choice for frozen solutions and powders.[22] Frozen solution ENDOR spectra consist of multiple overlapping powder patterns of different nuclei. To increase the resolution and determine the angles of the hfcc with respect to the *g*-tensor axes one has to

* Author to whom correspondence should be addressed. E-mail: lubitz@mpi-muelheim.mpg.de.
[†] Max-Planck-Institut für Bioanorganische Chemie.
[‡] Max-Planck-Institut für Medizinische Forschung.

10.1021/jp060548d CCC: $33.50
Published on Web 05/23/2006

selectively excite molecules that have different orientations with respect to the magnetic field. Since radical anions of quinones have a rhombic *g*-tensor one can select specifically oriented molecules by choosing a corresponding field position.[22] For a complete orientation selection all principal components of the *g*-tensor must be resolved. For the small *g*-anisotropy found in quinones, high-frequency EPR is necessary to resolve the *g*-tensor components. So far only few laboratories have utilized the advantage of high-frequency ENDOR for quinones.[23−26] For the isolated quinone radical anions studied here only X-band (∼9 GHz) ENDOR studies are available so far.[27−29]

Modern magnetic resonance spectroscopy receives great support from quantum chemical calculations. In particular density functional theory (DFT) has become an important tool for the calculation of spin Hamiltonian parameters.[30−32] Considering quinones, the calculation of *g*-tensors and ^{1}H hyperfine parameters is already well established in the literature.[33−38] In addition to quinone ring protons, the main focus of a recent theoretical study was the calculation of spectroscopic parameters of hydrogen bonds formed between solvent molecules and quinone radicals, which allows conclusions on the hydrogen-bond geometries.[26]

In this work we experimentally determined a complete set of the hfcc's of NQ, VK_3, and VK_1 semiquinone radical anions in alcoholic solution using pulsed ENDOR spectroscopy. The number of hydrogen bonds of the first solvent shell was determined using an EPR line shape analysis. Additionally, signals from nonexchangeable protons of the solvent were detected and analyzed. Furthermore, DFT was used to calculate the relevant structural and electronic parameters for the geometry-optimized systems. The effect of solvation was modeled in the calculations by using (i) the supermolecule approach to describe short-range interactions such as hydrogen bonding and (ii) the conductor-like screening approach (COSMO) to treat long-range solvation effects at low computational cost.[39] The agreement between DFT calculations and experiment is found to be very satisfying and clearly shows that even fine details of the electronic structure of such radicals can be reliably calculated by DFT methods. The study of these model systems presents a solid basis for a better understanding of the electronic structure of quinone radicals in solution. Furthermore, it is a mandatory prerequisite to understand the regulating effects of the protein on quinone cofactors.

Materials and Methods

Sample Preparation. 1,4-Benzoquinone (BQ), 1,4-naphthoquinone (NQ), 2-methyl-1,4-naphthoquinone (VK_3), and 2-methyl-3-phytyl-1,4-naphthoquinone (VK_1) were obtained commercially (Aldrich). The deuterated 1,4-benzoquinone (BQ-d_4) was prepared as described.[40] The degree of deuteration according to NMR and mass spectroscopy was better than 95%. 2-Methyl-1,4-naphthoquinone- (VK_3-d_8) was prepared as follows: 5 g of 2-methyl-naphthalene (Aldrich) was perdeuterated by heating with 100 mL of D_2O (99.9%) and 200 mg of Pt (Adams catalyst prereduced with deuterium gas) in a stainless steel high-pressure vessel with metal fittings for 8 days at 290 °C. The exchange was repeated twice under the same conditions. The final product was distilled in the bulb tube, yielding 9 g. Mass spectroscopy delivered $m/e = 152$, and the degree of deuteration was ∼98%. The freezing point was 34−36 °C. To 3.75 g of 2-methyl-naphthalene-d_{10} in 45 mL of CH_3COOD (90%, D_2O), 14.5 g of CrO_3 in 25 mL of diluted CH_3COOD (60%, D_2O) was added dropwise while stirring within 1 h. The temperature during the addition was kept at 5−10 °C, followed by room temperature for 30 min, then by heating at 40 °C for another hour. After being cooled, the mixture was poured in 200 mL of cold D_2O, filtered, washed with water, and recrystallized from ethanol/water. This yielded 1.5 g of crystalline product. Mass spectroscopy delivered $m/e = 172$, and the degree of deuteration was ∼98%. The melting point was determined to be 105−106 °C. The fully deuterated 1,4-naphthoquinone (NQ-d_6) was prepared from naphthalene-d_8 (Aldrich) as described above. 2-Propanol (IP)-h_8 and -d_8 were obtained from Merck (Darmstadt), and 2-propanol-d_1 was obtained from Roth (Karlsruhe).

Semiquinone radical anions for liquid solution measurements were prepared as follows: The respective quinone was dissolved in IP-h_8 and filled into the capillary (o.d. of 2 mm). The sample was connected to a high-vacuum line and pumped until all IP-h_8 was evaporated. IP-h_8 was degassed by three freeze−pump−thaw cycles on the line and was distilled in the sidearm on potassium *tert*-butylate, which was used as a base. Then the sample was frozen and evacuated again, degassed, and sealed under vacuum. The respective quinone was then dissolved in the solution of potassium *tert*-butylate in IP (concentration ∼0.2−0.5 mM) to generate the semiquinone radical anion. The use of benzyltrimethylammonium hydroxide ($C_{10}H_{17}ON$) (Lancaster, Newgate, U. K.) instead of potassium *tert*-butylate led to samples with identical EPR and ENDOR spectra.

Semiquinone radical anions for frozen solution measurements were generated using similar procedures described elsewhere.[25] The quinones were dissolved in IP, which was deoxygenated by bubbling with purified nitrogen in a quartz tube (o.d. of 3 mm). A small amount of a solution of benzyltrimethylammonium hydroxide in methanol was added to the deoxygenated solutions. Then, the samples were rapidly frozen in liquid nitrogen. The initial concentration of the quinones in IP was about 0.5 mM.

Spectroscopic Measurements. All experiments on frozen solutions were carried out at 80 K on a Bruker ELEXSYS E580-Q spectrometer with a Super Q-FT microwave bridge equipped with a home-built resonator similar to that in ref 41. Field-swept echo-detected (FSE) EPR spectra were recorded using the two-pulse echo sequence ($\pi/2-\tau-\pi-\tau-$echo), in which the echo intensity was registered as a function of the external magnetic field. Microwave (MW) pulses of 40 ns ($\pi/2$) and 80 ns (π pulse) and $\tau = 340$ ns were used. The ^{1}H ENDOR was recorded using the Davies ENDOR sequence[42] ($\pi-t-\pi/2-\tau-\pi-\tau-$echo) with an inversion π-pulse of 200 ns, $t = 21$ μs, radio frequency (RF) π-pulse of 17 μs, and the detection sequence similar to that of the FSE EPR experiment. The ^{2}H ENDOR was recorded using the Mims ENDOR sequence[43] ($\pi/2-\tau-\pi/2-t-\pi/2-\tau-$echo) with 44 ns $\pi/2$ pulses, $\tau = 268$ ns, and an RF π-pulse of 40 μs. An ENI 3200L (300 W) RF amplifier was used for ^{1}H ENDOR measurements, and an ENI A-500 (500 W) RF amplifier with a Trilithic high-power low-pass filter H4LE35-3-AA ("cut off" frequency of ∼35 MHz) for ^{2}H ENDOR measurements.

CW EPR and ENDOR measurements in liquid solution were performed on a Bruker ESP 300E X-band EPR spectrometer with home-built ENDOR accessories, consisting of a Rhode & Schwarz RF signal generator (type SMT 02) and an ENI A-500 (500 W) RF amplifier. A TM_{110}-type microwave cavity similar to the one described previously was used.[44] The sample temperature was controlled using a Bruker ER4111 VT nitrogen flow system.

EPR and ENDOR Simulations. The spin Hamiltonian for the case of an electron spin $S = {}^1/_2$ and nuclear spins I_i has the form

$$H = \mu_B \vec{B}_0 \mathbf{g} \vec{S} + \sum_{i=1}^{n} (-\mu_N^i g_N^i \vec{B}_0 \vec{I}_i + \vec{S}\mathbf{A}_i \vec{I}_i + \vec{I}_i \mathbf{Q}_i \vec{I}_i) \quad (1)$$

where B_0 is the external magnetic field, $\mathbf{g}$ is the electronic g-tensor, $\mathbf{A}_i$ and $\mathbf{Q}_i$ correspond to the hyperfine (hf) and quadrupole (nq) tensors of nucleus i, respectively, μ_B is the Bohr magneton, and μ_N and g_N are the nuclear magneton and g-factor of corresponding nuclei. For nuclei with spin $I = {}^1/_2$ the quadrupolar term in eq 1 is zero. The frequencies and probabilities of EPR and ENDOR transitions are derived from eq 1 by application of the selection rules $\Delta M_S = 1$ and $\Delta M_I = 0$ and $\Delta M_S = 0$ and $\Delta M_I = 1$ for allowed EPR and ENDOR transitions, respectively. Since paramagnetic centers of a frozen solution sample are randomly oriented, the EPR spectra are obtained by summation of signals from all orientations.

The ENDOR experiments are performed at a specific magnetic field. Due to the finite width of the microwave pulses, only part of the EPR spectrum is excited. In other words only the molecules with specific orientations relative to the magnetic field contribute to the ENDOR spectra. This effect (orientation selection) has to be taken into account to correctly estimate the impact of different transitions on the final ENDOR spectra.[22] At Q-band the magnitude of the hfcc of strongly coupled nuclei is comparable with the g-anisotropy. Thus, for a correct simulation of the EPR spectra, hfcc's of strongly coupled protons were included. The orientation selectivity of MW pulses in ENDOR was accounted for by (i) inclusion of the strongly coupled protons in the spin Hamiltonian and (ii) manual specification of the excitation width of pulses, comparable with the EPR line width. To increase the precision of the spin Hamiltonian parameter determination, both EPR and ENDOR simulations were done simultaneously.

All data processing and simulations were done in Matlab environment.[45] EPR and ENDOR spectra were simulated using the EasySpin software package (version 2.2.0).[46] This software directly evaluates the spin Hamiltonian without using any approximations. This, in particular, results in the correct calculation of orientation selectivity in ENDOR experiments, which is important for precise simulations. The ENDOR signatures of each nucleus were obtained separately and then summed with appropriate weight coefficients. A manual fit of experimental data was used in all cases. The effect of microwave pulse selectivity in Davies ENDOR experiments was taken into account by multiplication of the calculated ENDOR spectra with a frequency-dependent profile (self-ELDOR hole[47] (where ELDOR is electron−electron double resonance)) approximated by a Lorentzian function. The width (full width at half-height) of the profile was taken equal to $\Gamma_{ELDOR}/2\pi = 1/2t_{inv} = 2.5$ MHz. The efficiency of Mims ENDOR is hf-coupling-dependent (blind spots) and was calculated according to the simplified formula: $F(\nu - \nu_L) = {}^1/_2 \sin^2(2\pi(\nu - \nu_L)\tau)$, where ν_L is the nuclear Larmor frequency and $\tau = 268$ ns.[43,47]

Computational Details. Complete geometry optimizations were performed for $BQ^{\bullet-}$, $NQ^{\bullet-}$, $VK_3^{\bullet-}$, and $VK_1^{\bullet-}$, in coordination with two to four IP molecules. For $VK_1^{\bullet-}$ a reduced model system was employed, truncated after the fifth carbon of the phytyl chain. A starting conformation was chosen, in which the phytyl chain was oriented perpendicular to the ring plane. In each system, one or two hydrogen bonds to each carbonyl oxygen atom were assumed in the starting structures. The initial models contained in-plane hydrogen bonds. Furthermore, the solvent molecules were placed in such a way that the alkyl groups were located above and below the quinone planes. For $VK_3^{\bullet-}$ and $VK_1^{\bullet-}$, additional calculations were performed. For these, a special geometry optimization with hydrogen bonds restricted to the quinone plane was done. In all cases, the B3LYP density functional[48−50] was used in combination with the Dunning−Huzinaga basis sets, which were augmented by polarization and diffuse functions from the same authors.[51] The Gaussian 03 program was used for all geometry optimizations.[52] The spectroscopic data were computed in additional single-point calculations employing the optimized geometries. For this purpose the B3LYP functional was used in combination with the EPR-II basis set, which was developed for an accurate calculation of magnetic properties.[53] The g-values were calculated (using B3LYP/EPR-II) employing the coupled-perturbed Kohn−Sham equations,[31] in conjunction with a parametrized one-electron spin−orbit operator.[54−56] Magnetic hfcc's were calculated (B3LYP/EPR-II) for all hydrogen and deuterium atoms, including the isotropic Fermi contact terms and the dipolar hfcc's. All property calculations were performed employing the COSMO continuum method,[39] using the dielectric constant of $\epsilon = 18.3$ for IP. All spectroscopic data (g-tensors and hfcc's) were calculated with the program package ORCA.[57] Details of the implementation of the COSMO approach into the ORCA program and its application for the calculation of g-tensors can be found in a previous study.[58] Other groups have already demonstrated the strength of continuum models for the calculation of EPR parameters.[59−61] Alternatively, the usefulness of ensembles in ab initio molecular dynamics for modeling solvent effects was impressively demonstrated by Asher et al.[62]

Nomenclature and the Choice of the Coordinate System. All studied quinones have a planar structure of their ring(s). The x and y principal axes of the quinone g-tensor lie in the plane of the quinone; the x-direction is parallel to the C−O bonds; the z-direction is perpendicular to the quinone plane (Figure 1).[18] For all investigated model systems the angles of all tensors are given with respect to the g-frame. The relation between the coordinate systems of the hf and nq tensors and the g-coordinate system is given in spherical angles as shown in Figure 1. Positive values refer to a counterclockwise rotation.

Results and Discussion

EPR Spectra and *g*-Tensor Determination. The Q-band EPR spectra of $NQ^{\bullet-}$, $VK_3^{\bullet-}$, and $VK_1^{\bullet-}$ in IP-d_8 together with the orientation-selected ^{1}H ENDOR spectra are presented in Figure 1. For each case the EPR spectrum and selected ENDOR spectra, measured close to the canonical orientations of the g-tensor, are shown. The three field positions, at which the respective ENDOR spectra were measured (a, b, and c), are marked in the EPR spectrum. A number of additional experiments (a total of up to nine) were performed at other field positions to investigate the angular dependence of the hfcc's (data not shown). The simulations of the corresponding EPR and ENDOR spectra are presented by red lines. The simulated g-factors of the three radicals in IP-d_8 are given in Table 1. No difference was observed between g-factors of deuterated and nondeuterated compounds and for the differently deuterated solvents. The g-factors for $NQ^{\bullet-}$ and $VK_1^{\bullet-}$ are in agreement with earlier high-field EPR studies of nondeuterated compounds.[18]

Table 1 also presents the results of g-tensor calculations using DFT. All data from DFT calculations, unless otherwise stated, are taken from the corresponding models with four hydrogen bonds, which were optimized without restrictions. A detailed discussion of differences between models will be given below. While the g_y and g_z values are well predicted by the DFT

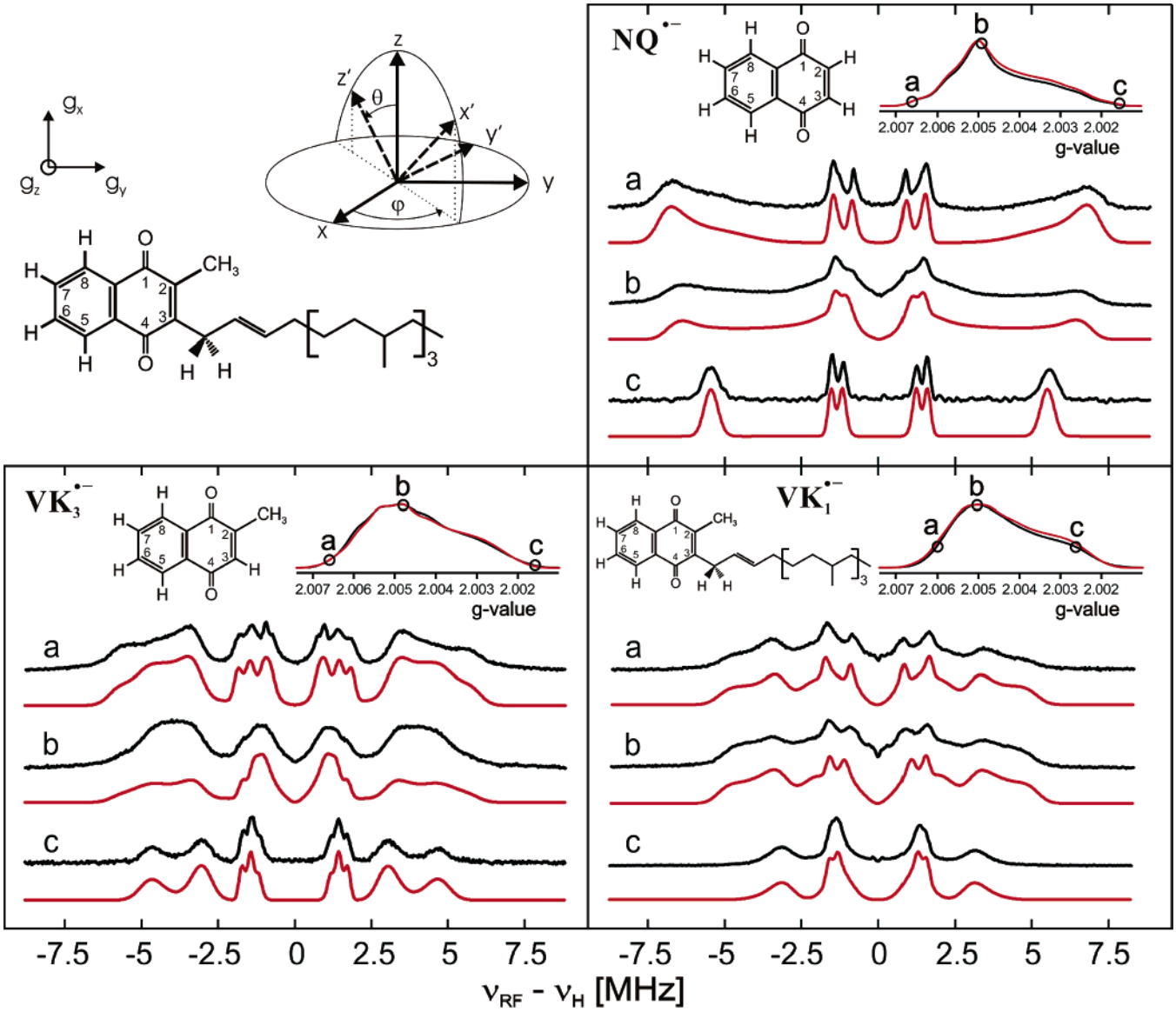

Figure 1. (Upper left panel) Molecular structure of VK_1 with numbering scheme. The principal axes of the *g*-tensor are shown (*x*, *y*, *z*). The *x* and *y* principal components lie in the plane of the quinone, and the *x*-direction is parallel to the C−O bonds; the *z*-direction is perpendicular to the quinone plane. This holds for all quinones investigated here. Hyperfine tensor angles are given with respect to the *g*-frame; the definitions of the respective spherical angles φ and θ are shown. Selected ^{1}H ENDOR spectra of $NQ^{\bullet-}$ (upper right panel), $VK_3^{\bullet-}$ (lower left panel), and $VK_1^{\bullet-}$ (lower right panel) in IP-d_8 recorded at $T = 80$ K and at different values of the magnetic field. The respective molecular structures with numbering schemes are given. ENDOR traces a, b, and c correspond to spectral positions near g_x, g_y, and g_z, respectively. The black trace for each position presents experimental data, and the red trace presents the simulation. The insets in the right corner show the field-swept echo-detected (FSE) EPR spectra and their simulations. The field positions, at which the presented ENDOR spectra are measured, are marked with letters. The parameters of ENDOR simulations (hfcc's and angles) are given in Tables 2−4.

calculations, the typical overestimation of the g_x component of quinone radicals was found. This discrepancy is on one hand the result of deficiencies in the present day density functionals.[33] On the other hand it was also shown that at least part of this discrepancy is due to insufficient model systems in the case of polar, protic solvents.[26] Increasing the amount of solvent molecules in the calculation and forming an extended solvent shell around the quinone leads to an improved prediction of the g_x values.[26,62] However, since the accurate prediction of *g*-factors is outside the scope of this article such time-consuming calculations were not performed.

The ENDOR spectra of quinones contain spectral features from a number of hydrogen nuclei that, for convenience of discussion, will be separated into three groups: (i) α-protons, directly attached to the π-system, and β-protons, one bond away from the π-system (Figure 1), (ii) protons hydrogen-bonded to the quinone oxygens, and (iii) protons from the solvent weakly coupled to the quinone.

Hyperfine Couplings: The Quinone Protons. ENDOR spectra of $NQ^{\bullet-}$, $VK_3^{\bullet-}$, and $VK_1^{\bullet-}$ in IP-d_8 as well as the spectral simulations are presented in Figure 1, and simulation parameters are summarized in Tables 2−4. To avoid signals from the protons of the solvent, completely deuterated 2-propanol (IP-d_8) was used for the measurements.

In $NQ^{\bullet-}$ protons at the positions 2/3, 5/8, and 6/7 are equivalent due to the symmetry of the molecule. Consequently, only three pairs of sharp lines are visible in the ENDOR spectra at "single-crystal-like" orientations close to g_x and g_z (traces a and c). The α-protons in positions 2 and 3 attached to the quinone ring have the largest hfcc's (see Figure S2 in the Supporting Information for spin density plots). The A_x (−14.00 MHz) and A_z (−11.20 MHz) principal components of their hf

TABLE 1: Principal Components of *g*-Tensors of $NQ^{\bullet-}$, $VK_3^{\bullet-}$, and $VK_1^{\bullet-}$ in IP-d_8 Derived from EPR Experiments at Q-Band at $T = 80$ K and Values from DFT Calculations[a]

	g_x	g_y	g_z	
$NQ^{\bullet-}$	2.00590(5)	2.00511(5)	2.00229(5)	this work[b]
	2.00582(5)	2.00505(5)	2.00228(5)	*c*
	2.00658	2.00530	2.00219	DFT
$VK_3^{\bullet-}$	2.00581(8)	2.00513(8)	2.00229(8)	this work[b]
	2.00638	2.00525	2.00215	DFT
$VK_1^{\bullet-}$	2.0057(1)	2.0051(1)	2.0023(1)	this work
	2.00566(5)	2.00494(5)	2.00216(5)	*c*
	2.00640	2.00526	2.00217	DFT

[a] Two solvent molecules were coordinated to each carbonyl oxygen. Geometry optimization was performed without restrictions. The *g*-factor calculations were performed using the ORCA program and employing the COSMO continuum method. [b] The *g*-tensor was obtained from fully deuterated quinones. [c] From a W-band EPR study (ref 18).

tensors are completely resolved while the A_y component (−1.76 MHz) overlaps with signals from benzene ring α-protons of $NQ^{\bullet-}$. The previous pulse[28] and CW[27] X-band studies showed very similar results but were less accurate. The principal components of the hf tensors of the protons in positions 6/7 exhibit the relation $|A_x| > |A_z| > |A_y|$, which is typical for α-protons of π-radicals.[63] Here, the direction of A_z is perpendicular to the quinone plane and A_y along the C−H bond. The presence of a large electron density on the carbonyl group strongly influences the hfcc's of protons at positions 5/8. For them the A_z component of the hf tensor is the largest. The DFT calculations show excellent agreement with the experimental data (Table 2).

In VK_3 the proton in position 2 is substituted with a methyl group (Figure 1, lower left panel). The rotational motion of the methyl group at 80 K completely averages the individual tensors of the methyl protons resulting in the observation of a single set for all three protons.[63] Thus, only two large couplings, from the methyl group protons and the α-proton at position 3, are observed. Since the substitution lowers the symmetry of the quinone molecule, four different couplings of protons 5−8 in the benzene ring are observed. The results of spectral simulations for the large hfcc's show good agreement with previous CW X-band studies,[27] while in other studies some hfcc's of the α-proton at position 3 were significantly overestimated (see, e.g., ref 28).

The experimental data and results of the DFT calculations are summarized in Table 3. The rotational averaging of the hfcc's of the methyl group was taken into account by averaging of the individual methyl proton tensors that were calculated in steps of 15° (the same procedure was applied for $VK_1^{\bullet-}$). The obtained average tensor is in excellent agreement with the experiment. The largest hfcc of the α-proton in position 3 is overestimated by approximately 10%. The other α-protons (benzene ring) are predicted with better precision.

VK_1 is even higher-substituted than VK_3 and carries a phytyl chain at position 3 (Figure 1, lower right panel). The protons of the first methylene group of the tail are expected to have quite large couplings. However, as noticed previously,[64] in frozen solution the position of the tail is not well-defined. Since the proton hfcc's are strongly dependent on the dihedral angle of the β-protons with respect to the quinone plane,[65] a broad distribution of hfcc's for these protons is expected. In agreement with this, the ENDOR spectra exhibit only three major features from the methyl group protons in position 2 and the benzene ring protons. Lines of protons in positions 5 and 8, and 6 and 7, are not resolved, which indicates a significantly decreased asymmetry of the electron spin density distribution compared to that of $VK_3^{\bullet-}$. DFT calculations show a similar precision of prediction of the hfcc's as in the case of $VK_3^{\bullet-}$ (Table 4). Earlier X-band studies of $VK_1^{\bullet-}$ [28,29] and its close structural analogue $MQ^{\bullet-}$ [10] yielded similar results for the strongly coupled protons.

The comparison between data obtained from ENDOR in liquid and frozen solution can be done by an analysis of the isotropic part of the hf tensor. In liquid solution the isotropic hfcc's are measured directly,[21] while in frozen solution the full hf tensor is measured and the isotropic part can be obtained from the trace of this tensor ($a_{iso} = {}^1/_3\mathrm{Tr}(\mathbf{A}) = {}^1/_3(A_x + A_y + A_z)$). Tables 2−4 present the isotropic hfcc's obtained in frozen and liquid solutions. The liquid solution data obtained in this work (for spectra see Figure S1 of the Supporting Information) agree very well with the data reported earlier.[27−29] Taking into account some minor changes of the hfcc's, which may be caused by freezing of the sample and the different temperatures (see, e.g., ref 64), very good agreement is found. This corroborates the line assignments made for the quinone protons in the present work.

Hyperfine Couplings: Hydrogen Bonds. Hydrogen bonds play an important role in the fine-tuning of the chemical properties of cofactors bound in proteins.[66] Thus, many studies addressed the elucidation of the related parameters from the EPR experiments and the determination of hydrogen-bond geometries; see, e.g., refs 25, 64, 67, and 68. Information on hydrogen bonds can be obtained from ENDOR spectroscopy, i.e., from ^{1}H or ^{2}H ENDOR on quinone radical anions in protonated or deuterated solvents, respectively. In the first case subtraction

TABLE 2: Parameters Used in the Fitting of ^{1}H ENDOR Spectra of $NQ^{\bullet-}$ in IP at $T = 80$ K (exptl) and Results of DFT Calculations[a]

	position[b]							
	2/3		5/8		6/7		hydrogen bond(s)	
	exptl	DFT	exptl	DFT	exptl	DFT	exptl	DFT (avg)
A_x	−14.00	−13.59	−1.69	−1.57	−3.12	−3.03	+5.68	+5.86
A_y	−1.76	−1.66	+0.36	+0.39	+0.19	+0.19	−2.70	−2.83
A_z	−11.15	−11.39	−3.17	−3.24	−2.40	−2.41	−2.70	−2.58
a_{iso}	−8.97	−8.88	−1.50	−1.47	−1.78	−1.75	<+0.1	+0.15
a_{iso}[c]	−9.07		−1.38		−1.82			
lw	0.6		0.22		0.24		0.5	
φ	±17	±17	±8	±8	±15	±15	±37, ±53	±37, ±53
θ	0	<2	0	<2	0	<2	<15	<4

[a] Two solvent molecules were coordinated to each carbonyl oxygen. Geometry optimization was performed without restrictions. Hyperfine tensor calculations were performed by employing the COSMO continuum method. Hyperfine couplings (A_i, a_{iso}) and line widths (lw, full width at half-height) are given in megahertz. Angles (φ and θ) are given in degrees. The precision of the hfcc determination is estimated to be 25% of the line width. The smallest component of the ring proton hfcc (A_y) exhibits a larger error. [b] Positions 2 and 3, 5 and 8, and 6 and 7 are equivalent. [c] Results obtained independently using CW ENDOR at X-band in liquid solution, $T = 280$ K (Figure S1, Supporting Information).

TABLE 3: Parameters Used in the Fitting of ^{1}H ENDOR Spectra of $VK_3^{\bullet-}$ in IP at $T = 80$ K (exptl) and Results of DFT Calculations[a]

	2 (CH_3)		3 (α)		5 (α)		6 (α)		7 (α)		8 (α)		hydrogen bond				
	exptl	DFT	exptl	DFT	exptl	DFT	exptl	DFT	exptl	DFT	exptl	DFT		I	II	III	IV
A_x	+6.40	+6.63	−11.73	−10.42	−1.48	−1.31	−3.80	−3.80	−3.01	−2.90	−1.99	−1.76	exptl	+5.5	+5.9	+6.3	+6.4
													DFT	+5.5	+5.9	+6.5	+6.7
A_y	+9.70	+10.10	−1.00	−0.78	+0.58	+0.60	+0.20	−0.07	+0.37	+0.29	+0.16	+0.05	exptl	−2.5	−2.8	−4.7	−4.1
													DFT	−2.5	−2.8	−4.7	−4.6
A_z	+5.80	+5.98	−9.60	−9.23	−3.00	−2.99	−2.82	−2.91	−2.34	−2.37	−3.54	−3.63	exptl	−2.4	−2.5	−4.9	−3.7
													DFT	−2.8	−2.5	−5.1	−4.5
a_{iso}	+7.30	+7.57	−7.44	−6.81	−1.30	−1.23	−2.14	−2.26	−1.66	−1.66	−1.79	−1.78	exptl	+0.2	+0.2	−1.1	−0.5
													DFT	<0.1	+0.2	−1.1	−0.8
a_{iso}[b]	+7.88		−7.16		−1.27		−2.10		−1.55		−1.81				n.d.		
lw	1.3		0.7		0.2		0.2		0.2		0.2				0.5		
φ	+25	+20	−21	−21	+4	+4	+12	+12	−20	−20	−14	−14	DFT	+48	−42	−58	+44
θ	0	<1	0	<3	0	<3	0	<3	0	<3	0	<3	DFT	<2	<2	−32	+21

[a] Two solvent molecules were coordinated to each carbonyl oxygen. Geometry optimization was performed without restrictions. Hyperfine tensor calculations were performed employing the COSMO continuum method. Hyperfine couplings (A_i, a_{iso}) and line widths (lw, full width at half-height) are given in megahertz. Angles (φ and θ) are given in degrees. The precision of the hfcc determination is 0.15 MHz for strongly coupled nuclei, 0.06 MHz for weakly coupled ring protons, and 0.2 MHz for hydrogen-bond protons. The precision of the hfcc determination is estimated to be 25% of the line width. The smallest component of the ring proton hfcc (A_y) exhibits a larger error. [b] Results obtained independently using CW ENDOR in the X-band in liquid solution, $T = 280$ K (Figure S1, Supporting Information). The assignment was done by comparison with DFT results.

TABLE 4: Parameters Used in the Fitting of ^{1}H ENDOR Spectra of $VK_1^{\bullet-}$ in IP at $T = 80$ K (exptl) and Results of DFT Calculations[a]

	2 (CH_3)		3 (CH_2)		5 (α)		6 (α)		7 (α)		8 (α)		hydrogen bond				
	exptl	DFT	exptl	DFT	exptl	DFT	exptl	DFT	exptl	DFT	exptl	DFT		I	II	III	IV
A_x	+6.40	+6.27		+0.41	−1.72	−1.50	−3.50	−3.52	−3.50	−3.42	−1.72	−1.52	exptl	+6.4	+6.1	+6.0	+5.5
				+3.39									DFT	+6.8	+6.6	+6.0	+6.0
A_y	+10.20	+9.57		+4.85	+0.50	+0.56	+0.04	+0.03	+0.04	+0.07	+0.50	+0.37	exptl	−5.2	−5.1	−4.0	−2.5
				+6.31									DFT	−5.2	−5.1	−4.0	−3.7
A_z	+6.05	+5.56		−0.76	−3.29	−3.20	−2.60	−2.75	−2.60	−2.69	−3.29	−3.26	exptl	−5.4	−5.3	−3.9	−2.2
				+2.63									DFT	−5.4	−5.3	−4.2	−3.6
a_{iso}	+7.55	+7.13		+1.50	−1.50	−1.39	−2.02	−2.08	−2.02	−2.01	−1.50	−1.47	exptl	−1.4	−1.4	−0.6	+0.3
				+4.11									DFT	−1.3	−1.3	−0.7	−0.4
a_{iso}[b]	+7.39		+2.45		−1.41		−2.12		−1.99		−1.54				n.d.		
			+4.50														
lw	0.7				0.2		0.2		0.2		0.2				0.5		
φ	+36	+34		−24	+10	+8	+16	+16	−17	−17	−10	−10	DFT	+59	−50	−51	+53
				−8													
θ	0	<1		−6	0	4	0	<1	0	<1	0	2	DFT	+57	−36	−26	+11
				+3													

[a] Two solvent molecules were coordinated to each carbonyl oxygen. Geometry optimization was performed without restrictions. Hyperfine tensor calculations were performed employing the COSMO continuum method. Hyperfine couplings (A_i, a_{iso}) and line widths (lw, full width at half-height) are given in megahertz. Angles (φ and θ) are given in degrees. When not specified parameters for simulations are taken from DFT calculations. The precision of the hfcc determination is estimated to be 25% of the linewidth. The smallest component of the ring proton hfcc (A_y) exhibits a larger error. [b] Results obtained independently using CW ENDOR in the X-band in liquid solution, $T = 220$ K (Figure S1, Supporting Information). The assignment was done by comparison with DFT results.

procedures are required to differentiate proton signals arising from the hydrogen bond, from the quinone molecule, and from the solvent. In earlier studies subtraction was typically done using ENDOR spectra of quinones in fully protonated and fully deuterated solvents. However, since we found that protons of the solvent, which are not involved in hydrogen bonds, also manifest themselves in the spectra, solvents selectively deuterated at the hydroxyl group (IP-d_1) were used as a reference in our analysis. In this case the difference of corresponding ENDOR spectra contains solely signals from the hydrogen bonds. To minimize subtraction artifacts deuterated quinones were used if available.

Figure 2 presents selected ^{1}H ENDOR spectra of BQ-$d_4^{\bullet-}$, NQ-$d_6^{\bullet-}$, and VK_3-$d_8^{\bullet-}$ in IP-d_1 (black traces) and difference spectra of the corresponding semiquinone radicals in IP-h_8 and IP-d_1 (blue traces). In the case of $VK_1^{\bullet-}$, for which no deuterated compound was available, the ^{1}H ENDOR difference spectra of the semiquinone radicals in IP-d_1 and IP-d_8 (black trace) as well as IP-h_8 and IP-d_1 (blue trace) are shown. Overall up to eight experiments at different field positions were performed. The

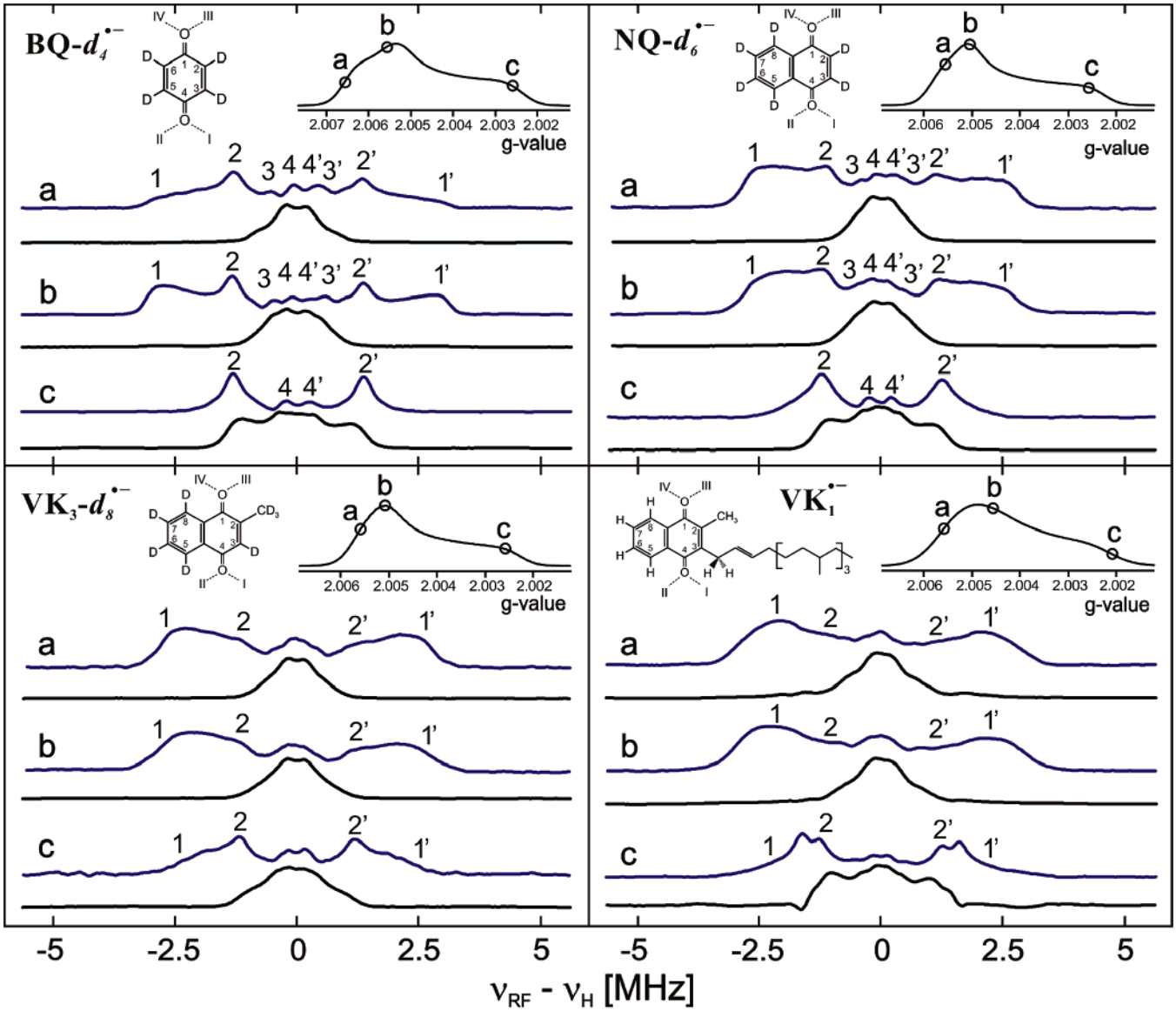

Figure 2. Selected ^{1}H ENDOR difference spectra in IP-h_8 and IP-d_1 (blue trace for each field position) and ^{1}H ENDOR spectra in IP-d_1 (black trace for each field position) of BQ-$d_4^{\bullet-}$ (upper left panel), NQ-$d_6^{\bullet-}$ (upper right panel), VK$_3$-$d_8^{\bullet-}$ (lower left panel), and VK$_1^{\bullet-}$ recorded at different values of the magnetic field. The molecular structures with numbering schemes are given. The hydrogen bonds are marked with Roman numbers. Traces a, b, and c correspond to spectral positions near g_x, g_y, and g_z, respectively. The ^{1}H ENDOR difference spectra show signals that stem only from the exchangeable protons. (These hydrogens form hydrogen bonds in a first and second solvation shell.) The spectra in IP-d_1 exhibit only nonexchangeable protons from the solvent. The inset in the right corner of each of the four panels shows the EPR spectrum. The field positions where the ENDOR experiments were done are marked with black circles and letters (a, b, and c). Specific spectral features (see text for discussion) are marked with Arabic numbers.

data for BQ-$d_4^{\bullet-}$ are included for comparison. The subtraction of ^{1}H ENDOR spectra of protonated quinones in IP-h_8 and IP-d_1 leads to comparable results (data not shown). However, it was found that difference spectra of deuterated compounds contain less subtraction artifacts.

The ^{1}H ENDOR difference spectra of BQ-$d_4^{\bullet-}$ are shown in Figure 2 (upper left plot, blue traces). A well-resolved dipolar powder pattern is observed. The magnetic dipolar interaction leads to an axially symmetric hf tensor. The largest component of the hf tensor lies along the hydrogen-bond direction. Previous studies found that for BQ$^{\bullet-}$ in alcoholic solvents the strongest component of the dipolar tensor lies in the plane of the quinone and is directed approximately along the lone pair orbitals of oxygen (53.5° from the C−O bond direction).[25] Therefore, it manifests itself in ^{1}H ENDOR spectra recorded near the spectral positions g_x and g_y (see lines 1 and 1′, traces a and b) but not near g_z (trace c). The small components of the axial tensor can be found in all ENDOR spectra (lines 2 and 2′ traces a, b, and c). Since only one dipolar pattern is observed we conclude that all hydrogen bonds to the quinone oxygens are equivalent. The simulation of the ENDOR spectra provides principal components of the hydrogen-bond tensor of $+6.25 \pm 0.05$, -2.90 ± 0.05, and -2.80 ± 0.05 MHz and an angle of $\varphi = 55 \pm 10°$, while the out-of-plane angle is below 10° (line width 0.3 MHz). These data are in full agreement with results of previous experimental studies[25,26] as well as previously published DFT calculations.[26,69] The length of the hydrogen bonds according to DFT calculations on BQ$^{\bullet-}$ in coordination with four IP molecules is 1.76 Å.

In all ENDOR difference spectra additional weak signals of exchangeable protons with couplings up to 1 MHz are observed (lines 3/3′ and 4/4′). We believe that these are not subtraction artifacts, since they are also visible in the difference spectra of protonated quinones, but rather signals from the hydrogen bonds of the second solvent shell. The principal components of their

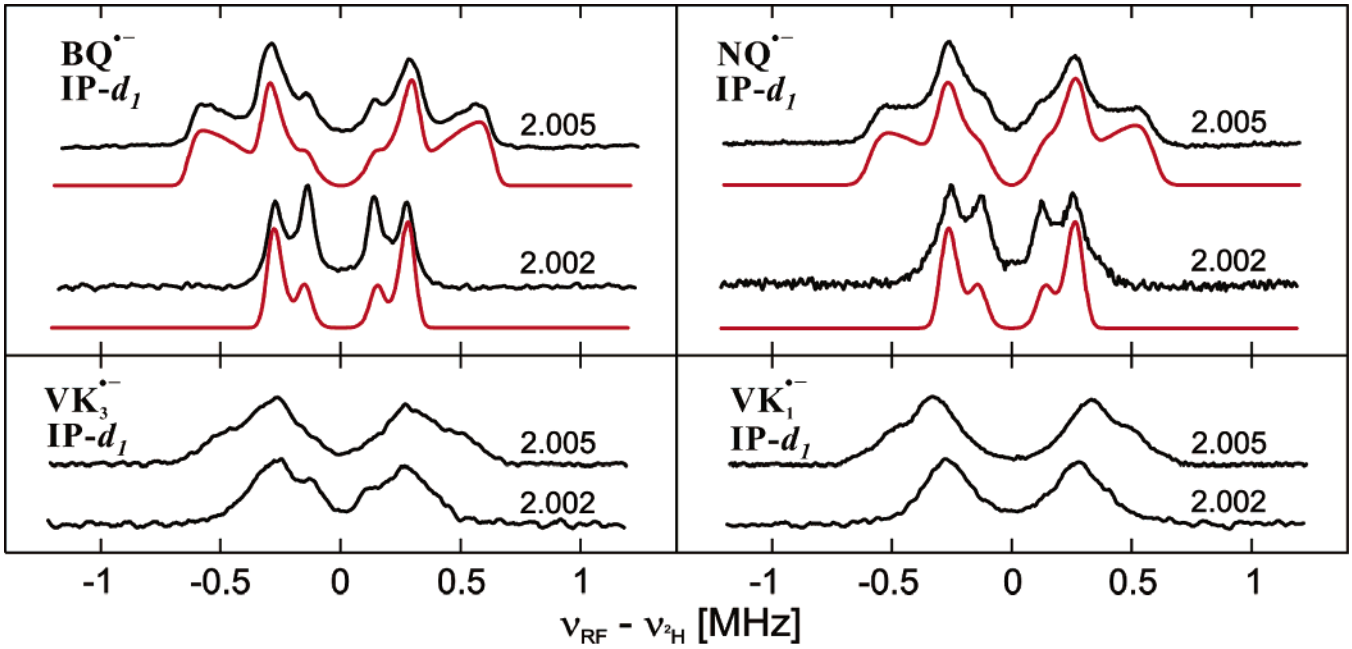

Figure 3. Deuterium Mims ENDOR spectra of $BQ^{\bullet-}$, $NQ^{\bullet-}$, $VK_3^{\bullet-}$, and $VK_1^{\bullet-}$ in IP-d_1 recorded at the peak maximum ($g \approx 2.005$) and at the high-field edge ($g \approx 2.002$) of the respective EPR spectra (shown in black). The simulations are shown in red. Simulation parameters for $BQ^{\bullet-}$ are: principal components of the hf tensor $A_x = +0.98 \pm 0.02$ MHz, $A_y = -0.47 \pm 0.02$ MHz, and $A_z = -0.44 \pm 0.01$ MHz and of the nq tensor $P_x = +102 \pm 10$ kHz, $P_y = -57 \pm 5$ kHz, and $P_z = -45 \pm 5$ kHz. The hf and nq tensors have the same orientation, $\varphi = 54 \pm 15°$, $\theta = 0°$. (See Figure 1 for the definition of angles.) Simulation parameters for $NQ^{\bullet-}$ are: principal components of hf tensor $A_x = +0.88 \pm 0.03$ MHz, $A_y = -0.40 \pm 0.03$ MHz, and $A_z = -0.41 \pm 0.01$ MHz and of the nq tensor $P_x = +102 \pm 12$ kHz, $P_y = -57 \pm 6$ kHz, $P_z = -45 \pm 6$ kHz. The hf and nq tensors are collinear ($\varphi = 54 \pm 15°$, $\theta = 0°$).

tensor are (+)1.06, (−)0.50, and (−)0.50 MHz, and the orientation of the tensor is similar to those of the hydrogen bonds. Provided that the weak hydrogen bonds are also established to the carbonyl oxygens, the length of the weak bond can be estimated to be approximately 1.8 times longer than those for the strong hydrogen bonds. This corresponds to a length of about 3.25 Å.

The ^{1}H ENDOR difference spectra of NQ-$d_6^{\bullet-}$ are similar to those of BQ-$d_4^{\bullet-}$. However, the line width of all spectral components is clearly increased (Figure 2, upper right panel). This indicates a certain distribution of hydrogen-bond parameters. Our DFT calculations predict that the in-plane angles of the two hydrogen bonds on the side of the benzene ring are changed while the orientations of the other two bonds are similar to those in $BQ^{\bullet-}$. However, a distribution of the in-plane angle φ cannot explain the loss of intensity of the A_y component in both ENDOR spectra recorded along the g_x and g_y directions. The simulation of the spectra (for simulation parameters see Table 2) shows that for the representation of spectral line shapes at least two of the hydrogen bonds should adopt an out-of-plane angle of up to 15°.

Kaupp et al.[33] have found that the results of structure optimizations of the quinones in alcoholic solvents using DFT depend on the starting conditions. The optimizations lead to multiple conformers with similar energies. These conformers differ by their out-of-plane angles of the hydrogen bonds between the quinone and the solvent molecules. For example, the $NQ^{\bullet-}$ structure reported by Kaupp et al.[33] has two hydrogen bonds with an out-of-plane angle of about 12° and two hydrogen bonds with 24°. The consequences of these flat potential surfaces are (i) a distribution of hydrogen-bond angles and (ii) a limited accuracy of the computed out-of-plane hydrogen-bond angles in the calculations.

The optimization of the molecular structure becomes even more problematic for the quinones with bulky substituents such as VK_3 (methyl group) and VK_1 (methyl group and phytyl tail). Here two different geometry optimizations were performed: (i) without any restrictions and (ii) with hydrogen bonds restricted to the plane of the quinone. The unrestricted structure optimization results in significant out-of-plane hydrogen bonding to the oxygen close to the bulky substituent. The DFT calculations showed that the couplings of ring protons were only marginally dependent on the geometry of the hydrogen bonds. In contrast, the hydrogen-bond hf tensors are strongly dependent on the hydrogen-bond out-of-plane angle and thus on the results of the geometry optimizations (Supporting Information, Tables S1 and S2).

The difference ^{1}H ENDOR spectra of VK_3-$d_8^{\bullet-}$ and $VK_1^{\bullet-}$ are presented in Figure 2 (bottom left and bottom right, respectively). The lines 2 and 2′ from the A_y component of the hf tensor become so broad that they almost disappear from the ENDOR spectra (traces a and b), and the wing of the large component of the dipolar coupling (lines 1 and 1′, trace c) becomes very prominent at the spectral position near g_z. Due to the poorly resolved spectra it is impossible to independently evaluate the hf parameters for each hydrogen bond. However, using the parameters obtained from DFT calculations on the model systems with four solvent molecules as starting values (Tables 3 and 4) we could achieve a reasonable ENDOR line shape simulation. Thereby, an indirect confirmation of the structure with nonplanar hydrogen bonds is obtained.

Figure 3 shows Mims ^{2}H ENDOR data on $BQ^{\bullet-}$, $NQ^{\bullet-}$, $VK_3^{\bullet-}$, and $VK_1^{\bullet-}$ in IP-d_1. Although these spectra contain only the lines from the deuterons of the hydrogen bond they are significantly more complicated than the ^{1}H ENDOR spectra due to the presence of nuclear quadrupole (nq) splitting. Only the $BQ^{\bullet-}$ and $NQ^{\bullet-}$ spectra are sufficiently resolved to deliver reliable simulations. The parameters of the simulations are given in the caption of Figure 3. Scaling the hfcc's of the deuterons by the factor γ^1_H/γ^2_H provided proton hfcc's close to those

derived from the ^{1}H ENDOR spectra. Similar hfcc's and nqcc's were recently determined experimentally for $BQ^{\bullet-}$.[25,26] The calculated nq couplings are somewhat larger than the experimental ones ($P_x = +115 \pm 2.5$, $P_y = -68 \pm 1$, $P_z = -47 \pm 1$ kHz both for $BQ^{\bullet-}$ and $NQ^{\bullet-}$). It was demonstrated for $BQ^{\bullet-}$ in H_2O that the inclusion of more than four water molecules in the solvation shell in the DFT calculations led to an additional reduction of the nqcc's.[26]

As observed for the proton ENDOR spectra (Figure 2), the deuterium ENDOR spectra of higher-substituted quinones exhibit a substantial broadening. Some splitting due to the nq interaction can still be observed in the ^{2}H ENDOR spectra of $VK_3^{\bullet-}$ at a field position close to g_z, while spectra of $VK_1^{\bullet-}$ do not show a resolved quadrupole splitting. This confirms that the hydrogen bonds show a larger disorder, and thus the spin Hamiltonian parameters are distributed.

However since the overall width of spectra does not change significantly upon addition of bulky substituents to the quinone molecule it can be concluded that the length of the hydrogen bond does not significantly change. This correlates with the results of the ^{1}H ENDOR where the distribution of hf parameters (primarily the out-of-plane angles) has been shown to be responsible for the ENDOR line broadening.

Length of the Hydrogen Bonds to the Quinone Radical Anions. In previous studies it was empirically established that the nq coupling constant $e^2qQ/h = 2P_{max}$ shows a linear dependence on the inverse third power of the length of the hydrogen bond[70,71]

$$e^2qQ/h = a - \frac{b}{r^3} \tag{2}$$

where a and b are empirical coefficients equal to 310 and 572[70] and 328 and 643,[71] respectively. P_{max} is the largest component of the nq coupling tensor (here P_x). The nq coupling constant is given in kilohertz, and the hydrogen-bond length in angstroms. Through the use of eq 2 and a nq coupling of $2P_{max} = 2P_x = 204$ kHz, a distance of 1.75 or 1.73 Å is obtained for both $BQ^{\bullet-}$ and $NQ^{\bullet-}$ for the two different sets of coefficients. Our DFT calculations with four solvent molecules showed that the hydrogen bonds have a length of 1.76−1.78 Å. These results correlate well with values of 1.74 Å for $BQ^{\bullet-}$ and 1.76−1.77 Å for $NQ^{\bullet-}$ obtained by Kaupp et al. [33] using DFT calculations.

Another experimental approach for the evaluation of the length of hydrogen bonds is based on the point-dipole model. From the dipolar part of the hf coupling the hydrogen-bond length can be calculated according to

$$A_{dip} = \frac{g_e\beta_e g_N\beta_N}{hr^3}\rho_S(3\cos^2\delta - 1) \tag{3}$$

where g_e and g_N are the electron and nuclear g-values, β_e and β_N are the electron and nuclear magnetons, ρ_S is the spin density at the quinone oxygen, δ is the angle between the applied magnetic field and the direction of the hydrogen bond, and r is the length of the hydrogen bond in angstroms.[22] The disadvantage of this approach is, however, that the spin density on the oxygen must be known for this estimation. This can be determined experimentally using ^{17}O labeling of the quinone and subsequent analysis of the oxygen hf coupling obtained from EPR experiments (see, e.g., refs 64, 72, and 73 for the analysis of $BQ^{\bullet-}$, $NQ^{\bullet-}$, and $VK_3^{\bullet-}$ in alcoholic solvents). However, it should be noted that the error of such an analysis can be quite large since only the largest component of the ^{17}O hf coupling is typically determined and a localization of the unpaired electron in the p_z orbital of the oxygen is assumed. The spin densities determined from experimental data are 0.23[64] for $BQ^{\bullet-}$ in IP, 0.20 for $NQ^{\bullet-}$ in ethanol,[72] and 0.19 for $VK_3^{\bullet-}$ in IP[73] (see Figure S2 of the Supporting Information for a comparison with calculated spin densities). ^{17}O hf couplings for $VK_1^{\bullet-}$ are not available; they should be very close to those of $VK_3^{\bullet-}$. Through the use of eq 3 and experimentally determined hfcc's of the hydrogen-bond protons, distances of 1.82, 1.78, and 1.78 Å are obtained for $BQ^{\bullet-}$, $NQ^{\bullet-}$, and the in-plane hydrogen bonds in $VK_3^{\bullet-}$. In view of the possible error margins of both methods, the agreement between the different methods of determination of hydrogen-bond length can be considered satisfying.

Number of Hydrogen Bonds to the Quinone Radical Anions. The number of hydrogen bonds cannot be directly determined from ENDOR spectra since the intensity of ENDOR lines is strongly dependent on nuclear relaxation and electron−nuclear cross relaxation times. However, taking into account that the line width of EPR spectra of quinone radical anions is significantly affected by the hyperfine interaction, it is possible to estimate the number of coupled nuclei from a careful analysis of the EPR spectral line width.[67] In fully deuterated quinones the hydrogen-bond protons are the strongest coupled nuclei; consequently their impact on the EPR line width is the largest. Hence, an analysis of the EPR line shape was done with deuterated quinones.

The analysis of the EPR line shapes was performed in three steps. In the first step the line width of the experimental EPR spectra of corresponding quinones in IP-d_1 was obtained. In the next step the simulation of EPR spectra using a spin Hamiltonian including hyperfine terms for two and four hydrogen bonds and the line width obtained in the first step was performed. Then, the effective line width of the simulated spectra was compared with the experimental EPR line width of quinones in IP-h_8.

The line widths of experimental spectra and effective line widths of simulated spectra were obtained in the following way. Since the line shape and intensity of pulsed EPR spectra are affected by various anisotropic relaxation effects, the standard deviation cannot be used as a criterion for the line width analysis of the simulation. Thus, we did not rely on the full simulation of pulsed EPR line shapes but tried to obtain the best agreement of the line width of each spectral component. The spin Hamiltonian with the electron Zeeman term was used (see Table 1 for simulated g-factors). The components of the spectra were broadened using anisotropic magnetic field strain as defined in the EasySpin package. The isotropic EPR line width was set to zero.

The magnetic field strain parameters for the experimental results and effective line width simulations are presented in Table 5. It can be seen that the line width of the EPR spectra increases with the number of hydrogen-bonded protons coupled to the radical. The simulations with two hydrogen bonds did not produce a broadening comparable with the EPR line width in IP-h_8 solvent for any of the quinones. However, four hydrogen bonds produce sufficient broadening (or even slight overbroadening) of the EPR lines. The case of three hydrogen bonds was excluded on the basis of our DFT calculations since such a situation yields very strong deviations of hfcc's of the ring protons from the experimentally determined ones (Supporting Information, Table S1). From this we conclude that four hydrogen bonds are present to the radicals in all cases ($BQ^{\bullet-}$, $NQ^{\bullet-}$, and $VK_3^{\bullet-}$). The number of hydrogen bonds to $VK_1^{\bullet-}$ was not analyzed since fully deuterated $VK_1^{\bullet-}$ was not available. Nevertheless, on the basis of our DFT calculations and taking into account the agreement of the experimentally determined

TABLE 5: Anisotropic Line Width Components (H_i) of EPR Spectra of BQ-$d_4^{\bullet-}$, NQ-$d_6^{\bullet-}$, and VK_3-$d_8^{\bullet-}$ in IP Solvents as Compared with EPR Line Widths from Simulations with Two or Four Hydrogen Bonds to the Carbonyl Oxygens[a]

quinone	solvent	H_x (MHz)	H_y (MHz)	H_z (MHz)
BQ-$d_4^{\bullet-}$	IP-d_8	7.8	5.5	7.3
	IP-d_1	8.8	7.9	9.4
	IP-h_8	**9.9**	**11.3**	**12.4**
	simulation with 2 H-bonds	8.9	9.0	11.5
	simulation with 4 H-bonds	**9.2**	**12.3**	**12.5**
NQ-$d_6^{\bullet-}$	IP-d_8	8.3	5.5	7.3
	IP-d_1	9.8	8.3	10.4
	IP-h_8	**11.4**	**9.8**	**11.6**
	simulation with 2 H-bonds	9.9	9.2	11.3
	simulation with 4 H-bonds	**10.2**	**10.3**	**12.1**
VK_3-$d_8^{\bullet-}$	IP-d_8	9.1	8.2	7.6
	IP-d_1	10.8	9.4	10.9
	IP-h_8	**11.4**	**11.6**	**12.2**
	simulation with 2 H-bonds	10.9	10.3	11.7
	simulation with 4 H-bonds	**11.3**	**11.6**	**12.4**

[a] See Tables 2−4 for the hfcc's of the hydrogen bonds. The precision of the line width determination is ~0.3 MHz.

hfcc's with those obtained theoretically, we predict four hydrogen bonds for $VK_1^{\bullet-}$ as well.

There is some contradiction in the literature concerning the number of hydrogen bonds that a semiquinone radical can have. Flores et al.[25,74] and Hales[67] experimentally determined two hydrogen bonds for $BQ^{\bullet-}$ in H_2O and for $BQ^{\bullet-}$ in methanol, respectively. The difference between these results and our estimation may be explained by (i) the impact of weakly coupled protons of the solvent (see next paragraph) that was not taken into account in previous studies and (ii) the fact that quinones in IP exhibit a smaller line width compared with H_2O and methanol that allows a more precise line width analysis.

The majority of previous DFT calculations of *g*- and hf-tensors on these and similar quinone radical anions also predicts the formation of four hydrogen bonds (see, e.g., refs 26 and 33). As mentioned above, our DFT calculations clearly support this view by a comparison of measured and calculated hfcc's obtained for different model systems (see also the Supporting Information, Tables S1 and S2).

Hyperfine Couplings of Weakly Coupled Protons of the Solvent. The presence of a so-called matrix line from distant nuclei is common for ENDOR spectra of frozen samples.[20,22,75] The matrix line is centered at the Larmor frequency and is typically not or only weakly structured. However, in our ^1H ENDOR spectra of fully deuterated quinone radical anions in IP-d_1 a clearly resolved structure was found.

The ^1H ENDOR spectra of BQ-$d_4^{\bullet-}$, NQ-$d_6^{\bullet-}$, and VK_3-$d_8^{\bullet-}$ in IP-d_1 are presented in Figure 2, lower trace, for each field position. These spectra arise from nonexchangeable bulk-solvent protons since in IP-d_1 the hydroxyl group is deuterated. ^1H ENDOR spectra of BQ-$d_4^{\bullet-}$, NQ-$d_6^{\bullet-}$, and VK_3-$d_8^{\bullet-}$ in fully deuterated IP (not shown) exhibit extremely weak signals mainly due to the incompletely deuterated quinones. In this way the contribution of quinone protons and protons of benzyltrimethylammonium hydroxide, used to produce the radical anion, to the ENDOR spectra of respective quinone radical anions in IP-d_1 can be excluded.

Several previous investigations, in which a subtraction of quinone ENDOR spectra in IP-h_8 and IP-d_8 was used for the analysis of hydrogen bonds, attributed these solvent signals to a second set of weaker hydrogen bonds. Our results do not support this assignment. Also it is interesting to notice that in contrast to the hydrogen-bond signals, which are presented in the same figures (see upper trace for each field position), the hf tensors of these solvent protons have a different orientation. While the largest component of the hydrogen-bond tensors lies in the plane of the quinone (at least for $BQ^{\bullet-}$ and $NQ^{\bullet-}$) the corresponding largest component of the bulk-solvent protons is oriented nearly perpendicular to this plane. It should be noted that at orientations close to g_z the lines from weakly coupled protons and hydrogen-bond protons overlap. The simulations give values of 2.1−2.4 MHz for the largest component of this hf tensor and 1.0−1.2 MHz for the smaller one.

Assuming a primarily dipolar nature of the interaction of these nuclei with the unpaired electron, the position of the proton must be above or below the quinone plane (carbonyl oxygens). In this case the largest component of the hyperfine tensor will be perpendicular to the π-plane, as observed in the experiment. The strength of a dipolar interaction is dependent on the distance of the nucleus to the unpaired electron (see eq 3). To estimate the maximum distance of the observed solvent shell protons, we used DFT and calculated the dependence of the hyperfine coupling of a proton from a methane molecule located straight above the carbonyl oxygen on the distance from the plane. The oxygen carries the largest electron spin density, and thus the corresponding distance is the longest. According to these calculations a proton that is located 3.1 Å above the carbonyl oxygen will have the largest hf component of $A_{||} = +2.3$ MHz. This result, however, has to be considered only as a crude estimate.

The number of weakly coupled protons can be estimated using a method analogous to that used for the hydrogen bonds. The EPR spectral line width of quinone radical anions in IP-d_8 is used as a reference. Then a number of hf tensors (with parameters estimated from ENDOR measurements) is added to the Hamiltonian to obtain the line width of the EPR spectra of the quinone radical anion in IP-d_1. The estimation (not shown) gives about four weak couplings for $BQ^{\bullet-}$, four to six couplings for $NQ^{\bullet-}$, and six to eight couplings for $VK_3^{\bullet-}$. Since the couplings of all protons are not necessarily the same, a quite large error in the determination of the amount of protons can be expected.

There are two possible assignments of the small solvent proton couplings: (i) to the protons of the hydrogen-bonded solvent molecules and (ii) to the protons of other solvent molecules, which are located above (below) the quinone plane. The optimized structures with four hydrogen bonds give a closest distance to the methyl group protons of about 2.9 Å and an angle of the largest hf component from g_z of about 15°. However at 80 K we expect free rotation of the methyl groups, which leads to an averaging of hf couplings of the methyl group protons. Since the other protons of the methyl group are further away from the oxygen, the average hfcc is expected to be smaller than the one observed experimentally. In addition, similar hfcc's from the solvent have been observed by us for $BQ^{\bullet-}$ in aprotic solvents, which do not form hydrogen bonds. The CH protons of hydrogen-bonded IPs are more than 3.3 Å away from the oxygen, and their out-of-plane angles are about 50°. This suggests that the second assignment is more likely.

Conclusions

In this work the semiquinone radical anions $BQ^{\bullet-}$, $NQ^{\bullet-}$, $VK_3^{\bullet-}$, and $VK_1^{\bullet-}$ in frozen 2-propanol solution were measured using pulsed Q-band ENDOR spectroscopy. The use of a higher microwave frequency band (34 GHz) than conventional X-band allowed us to improve the orientation selection and to determine the hf tensor principal components for all protons in the ENDOR spectra.

Special attention was paid to the determination of the number, strength, and geometry of hydrogen bonds formed between the quinone radical anions and specific solvent molecules in frozen solution. We confirmed the hypothesis of the presence of two strong hydrogen bonds to each oxygen of the semiquinone radicals and found that in $VK_3^{\bullet-}$ and $VK_1^{\bullet-}$ some of these hydrogen bonds do not lie in the plane of the quinone. This spread of hydrogen-bond geometries turned out to be the major problem in the analysis of ENDOR spectra. In addition to the strong hydrogen bonds, signals from the weaker coupled exchangeable protons from a second solvation shell were identified. It can be speculated that these protons are part of a solvent hydrogen-bond network and are located in the plane of the quinone close to the quinone oxygens.

Hydrogen-bond lengths were estimated both from the dipolar coupling of the respective protons using the point-dipole model and from nuclear quadrupole couplings using empirical formulas.[70,71] The distances obtained by these two methods are similar with the latter one in better agreement with the geometry obtained from the DFT calculations. The hydrogen-bond lengths to the investigated immobilized radicals all lie in the same range around 1.77 ± 0.05 Å. In an earlier study on $BQ^{\bullet-}$ similar hydrogen-bond lengths were found for different alcoholic solvents and water.[25]

Furthermore, resonances of weakly coupled nonexchangeable protons of the solvent were detected. The analysis of the respective hfcc's suggests that these protons are located above and below the quinone plane, e.g., close to the carbonyl groups that carry the majority of the spin density. These probably belong to the hydrogen-bonded solvent molecules or to additional solvent molecules located above or below the π-plane of the radical.

Several theoretical studies have already been devoted to the calculation of spin Hamiltonian parameters of quinone radicals, but only a few reported the hfcc's of the ring protons.[28,29,76] The results of these studies for naphthoquinone radical anions were compared mostly with the isotropic hfcc's available in the literature. In our work a more extensive comparison was performed, since all proton hyperfine tensors have been determined.

Our DFT calculations demonstrated the potential of the method in predicting the hf tensors of the quinone protons. The error of prediction increases with the complexity of the model but does not exceed 15%. Hyperfine tensor orientations could also be predicted by the calculations and were found to be helpful in the spectral simulations. The calculations showed that four hydrogen-bonded solvent molecules are necessary to obtain the best agreement with the experiments. The combination with a COSMO continuum model further improved the agreement with the experimental results.

The results of this study form a solid basis for the analysis of EPR and ENDOR data of VK_1 and MQ radicals in biological systems. The accurate set of hyperfine data, obtained here for the VK_1 radical anion in vitro, is very important for a solid comparison with data obtained for this radical in redox proteins. By such a comparison a deeper understanding can be achieved of how the protein surrounding tunes the electronic structure and the physical properties of this molecule, e.g., in photosystem I of oxygenic photosynthesis.

Acknowledgment. The authors acknowledge C. Laurich for the sample preparation, I. Heise for the deuteration of benzoquinone, and G. Klihm (all MPI Mülheim) for help with the CW EPR and ENDOR experiments. We thank M. Flores (MPI Mülheim) for helpful discussions. This work has been supported by the Max Planck Society.

Supporting Information Available: Liquid solution CW ENDOR spectra, from which the isotropic hfcc's were derived, the unpaired electron spin density population over $NQ^{\bullet-}$, $VK_3^{\bullet-}$, and truncated $VK_1^{\bullet-}$, comparison of the spin Hamiltonian parameters for $VK_3^{\bullet-}$ and $VK_1^{\bullet-}$ as determined experimentally and calculated using DFT for different model systems, and the coordinates of geometry-optimized structures of $NQ^{\bullet-}$, $VK_3^{\bullet-}$, and truncated $VK_1^{\bullet-}$ coordinated with four IP molecules. This material is available free of charge via the Internet at http://pubs.acs.org.

References and Notes

(1) *Vitamin K and Vitamin K-Dependent Proteins: Analytical, Physiological, and Clinical Aspects*; CRC Press: Boca Raton, FL, 1993.
(2) Blankenship, R. E. *Molecular Mechanisms of Photosynthesis*, 1st ed.; Blackwell Science: Oxford, U. K., 2002.
(3) Trumpower, B. L. *Function of Quinones in Energy Conserving Systems*; Academic Press: New York, 1982.
(4) Voet, D.; Voet, J. D. *Biochemistry*, 3rd ed.; Wiley: New York, 2004.
(5) Jordan, P.; Fromme, P.; Witt, H. T.; Klukas, O.; Saenger, W.; Krauss, N. *Nature* **2001**, *411* (6840), 909−917.
(6) Imhoff, J. F.; Bias-Imhoff, U. Lipids, Quinones and Fatty Acids of Anoxygenic Phototrophic Bacteria. In *Anoxygenic Photosynthetic Bacteria*; Blankenship, R. E., Madigan, M. T., Bauer, C. E., Eds.; Kluwer Academic Publishers: Dordrecht, The Netherlands, 1995; pp 179−205.
(7) Thurnauer, M. C.; Brown, J. W.; Gast, P.; Feezel, L. L. *Radiat. Phys. Chem.* **1989**, *34* (4), 647−651.
(8) Van der Est, A. *Biochim. Biophys. Acta* **2001**, *1507* (1−3), 212−225.
(9) Rigby, S. E. J.; Evans, M. C. W.; Heathcote, P. *Biochim. Biophys. Acta* **2001**, *1507* (1−3), 247−259.
(10) Gardiner, A. T.; Zech, S. G.; MacMillan, F.; Käss, H.; Bittl, R.; Schlodder, E.; Lendzian, F.; Lubitz, W. *Biochemistry* **1999**, *38* (36), 11773−11787.
(11) Lubitz, W.; Feher, G. *Appl. Magn. Reson.* **1999**, *17* (1), 1−48.
(12) Brettel, K. *Biochim. Biophys. Acta* **1997**, *1318* (3), 322−373.
(13) Brettel, K.; Leibl, W. *Biochim. Biophys. Acta* **2001**, *1507* (1−3), 100−114.
(14) Bittl, R.; Zech, S. G. *Biochim. Biophys. Acta* **2001**, *1507* (1−3), 194−211.
(15) Feher, G.; Okamura, M. Y. *Appl. Magn. Reson.* **1999**, *16*, 63−100.
(16) Feher, G. *Appl. Magn. Reson.* **1998**, *15*, 23−38.
(17) Pushkar, Y. N.; Golbeck, J. H.; Stehlik, D.; Zimmermann, H. *J. Phys. Chem. B* **2004**, *108* (27), 9439−9448.
(18) Burghaus, O.; Plato, M.; Rohrer, M.; Möbius, K.; MacMillan, F.; Lubitz, W. *J. Phys. Chem.* **1993**, *97* (29), 7639−7647.
(19) Teutloff, C.; Hofbauer, W.; Zech, S. G.; Stein, M.; Bittl, R.; Lubitz, W. *Appl. Magn. Reson.* **2001**, *21* (3−4), 363−379.
(20) Kevan, L.; Kispert, L. D. *Electron Spin Double Resonance Spectroscopy*; John Wiley and Sons: New York, 1976.
(21) Kurreck, H.; Kirste, B.; Lubitz, W. *Electron Nuclear Double Resonance Spectroscopy of Radicals in Solution—Applications to Organic and Biological Chemistry*; VCH Publishers: Deerfield Beach, FL, 1988.
(22) Schweiger, A.; Jeschke, G. *Principles of Pulse Electron Paramagnetic Resonance*; Oxford University Press: New York, 2001.
(23) Rohrer, M.; Prisner, T. F.; Vrieze, B.; Möbius, K.; Gardiner, A.; Lendzian, F.; Lubitz, W. *Biophys. J.* **1997**, *72* (2), TH422.
(24) Rohrer, M.; Plato, M.; MacMillan, F.; Grishin, Y.; Lubitz, W.; Möbius, K. *J. Magn. Reson. A* **1995**, *116* (1), 59−66.
(25) Flores, M.; Isaacson, R.; Calvo, R.; Feher, G.; Lubitz, W. *Chem. Phys.* **2003**, *294*, 401−413.
(26) Sinnecker, S.; Reijerse, E.; Neese, F.; Lubitz, W. *J. Am. Chem. Soc.* **2004**, *126*, 3280−3290.
(27) MacMillan, F. Doctoral Thesis, Freie Universität Berlin, 1993.
(28) Teutloff, C. Doctoral Thesis, Technische Universität Berlin, 2003.
(29) Teutloff, C.; Bittl, R.; Lubitz, W. *Appl. Magn. Reson.* **2004**, *26*, 5−21.
(30) Koch, W.; Holthausen, M. C. *A Chemist's Guide to Density Functional Theory*; Wiley-VCH: Weinheim, Germany, 2001.
(31) Neese, F. *J. Chem. Phys.* **2001**, *115* (24), 11080−11096.
(32) Kaupp, M. *Calculation of NMR and EPR Parameters—Theory & Applications*; Wiley-VCH: Weinheim, Germany, 2004.
(33) Kaupp, M.; Remenyi, C.; Vaara, J.; Malkina, O. L.; Malkin, V. G. *J. Am. Chem. Soc.* **2002**, *124* (11), 2709−2722.

(34) Mattar, S. M. *J. Phys. Chem. B* **2004**, *108* (27), 9449−9455.
(35) O'Malley, P. J. *Antioxid. Redox Signaling* **2001**, *3* (5), 825−838.
(36) Chipman, D. M. *J. Phys. Chem. A* **2000**, *104* (50), 11816−11821.
(37) Mattar, S. M.; Emwas, A. H.; Stephens, A. D. *Chem. Phys. Lett.* **2002**, *363* (1−2), 152−160.
(38) Eriksson, L. A.; Himo, F.; Siegbahn, P. E. M.; Babcock, G. T. *J. Phys. Chem. A* **1997**, *101* (49), 9496−9504.
(39) Klamt, A.; Schüürmann, G. *J. Chem. Soc., Perkin Trans. 2* **1993**, 799−805.
(40) Zhao, X. J.; Imahori, H.; Zhan, C. G.; Sakata, Y.; Iwata, S.; Kitagawa, T. *J. Phys. Chem. A* **1997**, *101* (4), 622−631.
(41) Sienkiewicz, A.; Smith, B. G.; Veselov, A.; Scholes, C. P. *Rev. Sci. Instrum.* **1996**, *67* (6), 2134−2138.
(42) Davies, E. R. *Phys. Lett. A* **1974**, *47* (1), 1−2.
(43) Mims, W. B. *Proc. R. Soc. London, Ser. A* **1965**, *283* (1395), 452−457.
(44) Zweygart, W.; Thanner, R.; Lubitz, W. *J. Magn. Reson. A* **1994**, *109* (2), 172−176.
(45) *Matlab*; The Mathworks, Inc.: Natick, MA, 2004
(46) Stoll, S.; Schweiger, A. *J. Magn. Reson.* **2005**, *177* (2), 390−403.
(47) Gemperle, C.; Schweiger, A. *Chem. Rev.* **1991**, *91*, 1481−1505.
(48) Lee, C. T.; Yang, W. T.; Parr, R. G. *Phys. Rev. B* **1988**, *37* (2), 785−789.
(49) Becke, A. D. *J. Chem. Phys.* **1993**, *98* (7), 5648−5652.
(50) Stephens, P. J.; Devlin, F. J.; Chabalowski, C. F.; Frisch, M. J. *J. Phys. Chem.* **1994**, *98* (45), 11623−11627.
(51) Dunning, T. H. *J. Chem. Phys.* **1970**, *53* (7), 2823−2833.
(52) Frisch, M. J.; Trucks, G. W.; Schlegel, H. B.; Scuseria, G. E.; Robb, M. A.; Cheeseman, J. R.; Montgomery, J. A., Jr.; Vreven, T.; Kudin, K. N.; Burant, J. C.; Millam, J. M.; Iyengar, S. S.; Tomasi, J.; Barone, V.; Mennucci, B.; Cossi, M.; Scalmani, G.; Rega, N.; Petersson, G. A.; Nakatsuji, H.; Hada, M.; Ehara, M.; Toyota, K.; Fukuda, R.; Hasegawa, J.; Ishida, M.; Nakajima, T.; Honda, Y.; Kitao, O.; Nakai, H.; Klene, M.; Li, X.; Knox, J. E.; Hratchian, H. P.; Cross, J. B.; Bakken, V.; Adamo, C.; Jaramillo, J.; Gomperts, R.; Stratmann, R. E.; Yazyev, O.; Austin, A. J.; Cammi, R.; Pomelli, C.; Ochterski, J. W.; Ayala, P. Y.; Morokuma, K.; Voth, G. A.; Salvador, P.; Dannenberg, J. J.; Zakrzewski, V. G.; Dapprich, S.; Daniels, A. D.; Strain, M. C.; Farkas, O.; Malick, D. K.; Rabuck, A. D.; Raghavachari, K.; Foresman, J. B.; Ortiz, J. V.; Cui, Q.; Baboul, A. G.; Clifford, S.; Cioslowski, J.; Stefanov, B. B.; Liu, G.; Liashenko, A.; Piskorz, P.; Komaromi, I.; Martin, R. L.; Fox, D. J.; Keith, T.; Al-Laham, M. A.; Peng, C. Y.; Nanayakkara, A.; Challacombe, M.; Gill, P. M. W.; Johnson, B.; Chen, W.; Wong, M. W.; Gonzalez, C.; Pople, J. A. *Gaussian 03*, revision B.01; Gaussian, Inc.: Wallingford, CT, 2004.
(53) Barone, V. *Recent Advances in Density Functional Methods*; World Scientific: Singapore, 1996.
(54) Koseki, S.; Schmidt, M. W.; Gordon, M. S. *J. Phys. Chem.* **1992**, *96* (26), 10768−10772.
(55) Koseki, S.; Gordon, M. S.; Schmidt, M. W.; Matsunaga, N. *J. Phys. Chem.* **1995**, *99* (34), 12764−12772.
(56) Koseki, S.; Schmidt, M. W.; Gordon, M. S. *J. Phys. Chem. A* **1998**, *102* (50), 10430−10435.
(57) Neese, F. *ORCA. an ab initio, Density Functional and Semiempirical Program Package*, version 2.4; Max-Planck-Institut für Bioanorganische Chemie: Mülheim an der Ruhr, Germany, 2004
(58) Sinnecker, S.; Rajendran, A.; Klamt, A.; Diedenhofen, M.; Neese, F. *J. Phys. Chem. A* **2006**, *110* (6), 2235−2245.
(59) Rinkevicius, Z.; Telyatnyk, L.; Vahtras, O.; Ruud, K. *J. Chem. Phys.* **2004**, *121* (11), 5051−5060.
(60) Ciofini, I.; Adamo, C.; Barone, V. *J. Chem. Phys.* **2004**, *121* (14), 6710−6718.
(61) Ciofini, I.; Reviakine, R.; Arbuznikov, A.; Kaupp, M. *Theor. Chem. Acc.* **2004**, *111* (2−6), 132−140.
(62) Asher, J. R.; Doltsinis, N. L.; Kaupp, M. *J. Am. Chem. Soc.* **2004**, *126* (31), 9854−9861.
(63) Carrington, A.; McLachlan, A. D. *Introduction to Magnetic Resonance*; Harper & Row: New York, 1969.
(64) MacMillan, F.; Lendzian, F.; Lubitz, W. *Magn. Reson. Chem.* **1995**, *33*, S81−S93.
(65) Heller, C.; McConnell, H. M. *J. Chem. Phys.* **1960**, *32* (5), 1535−1539.
(66) Jeffrey, G. A.; Saenger, W. *Hydrogen Bonding in Biological Structures;* 2nd ed.; Springer-Verlag: Berlin, 1994.
(67) Hales, B. J. *J. Am. Chem. Soc.* **1976**, *98*, 7350−7357.
(68) Rohrer, M.; MacMillan, F.; Prisner, T. F.; Gardiner, A. T.; Möbius, K.; Lubitz, W. *J. Phys. Chem. B* **1998**, *102* (23), 4648−4657.
(69) O'Malley, P. J. *J. Phys. Chem. A* **1997**, *101* (50), 9813−9817.
(70) Soda, G.; Chiba, T. *J. Chem. Phys.* **1969**, *50* (1), 439−455.
(71) Hunt, M. J.; Mackay, A. L. *J. Magn. Reson.* **1974**, *15* (3), 402−414.
(72) Broze, M.; Luz, Z.; Silver, B. L. *J. Chem. Phys.* **1967**, *46* (12), 4891−4902.
(73) Pushkar, Y. N.; Ayzatulin, O.; Stehlik, D. *Appl. Magn. Reson.* **2005**, *28* (3−4), 195−211.
(74) Flores, M.; Isaacson, R.; Lubitz, W.; Feher, G. *Biophys. J.* **2003**, *84* (2), 120A.
(75) Astashkin, A. V.; Kawamori, A. *J. Magn. Reson.* **1998**, *135* (2), 406−417.
(76) O'Malley, P. J. *Biochim. Biophys. Acta* **1999,** *1411* (1), 101−113.